

Supporting Information for
Multi method approach for analysis of road dust particles: elemental ratios,
SP-ICP-TOF-MS, and TEM

Feiyun Tou¹, Md. Mahmudun Nabi², Jingjing Wang², Mahdi Erfani³, Erfan Goharian³, Jing Chen,⁴ Yi Yang^{1*},
and Mohammed Baalousha^{2*}

¹ *Key Laboratory of Geographic Information Science (Ministry of Education), School of Geographical Sciences, East China Normal University, 500 Dongchuan Road, Shanghai 200241, China*

² *Center for Environmental Nanoscience and Risk, Department of Environmental Health Sciences, Arnold School of Public Health, University of South Carolina, Columbia, South Carolina, 29201, United State*

³ *Department of Civil and Environmental Engineering, University of South Carolina, SC 29208, USA*

⁴ *State Key Laboratory of Estuarine and Coastal Research, Yangtze Delta Estuarine Wetland Ecosystem Observation and Research Station, Ministry of Education & Shanghai, East China Normal University, 3663 North Zhongshan Road, Shanghai 200062, China*

*** Corresponding Author**

Yi Yang - *Key Laboratory of Geographic Information Science (Ministry of Education); School of Geographical Sciences, East China Normal University, 500 Dongchuan Road, Shanghai 200241, China; Phone: +86-21-54341196; Email: yyang@geo.ecnu.edu.cn*

Mohammed Baalousha - *Center for Environmental Nanoscience and Risk, Department of Environmental Health Sciences, Arnold School of Public Health, University of South Carolina, Columbia, South Carolina, 29201, United State; Phone: +1-803-777-7177; Email: mbaalous@mailbox.sc.edu*

Table S1 Parameters of ICP-MS and SP-ICP-TOF-MS.

Instrument Parameter	ICP-MS	SP-ICP-TOF-MS
Nebulizer Gas Flow	0.85 to 1 L/min	1.10 to 1.14 L/min
Auxiliary Gas Flow	1.02 L/min	0.8 L/min
Plasma Gas Flow	16 L/min	14 L/min
ICP RF Power	1600 W	1550 W
Analog Stage Voltage	-1600 V	--
Pulse Stage Voltage	1600 V	--
Discriminator Threshold	12	--
Deflector Voltage	-9.5 V	--
Dwell time	50 ms	--
Sample Flow Rate	0.3 mL/min	0.4 mL/min
Collision Cell Gas	--	Helium with 4.5% Hydrogen
Collision Cell Gas Flow	--	5.0 mL/min
Integration Time	--	2 ms
Transport Efficiency	--	5-7%
Detected mass range	--	14-275 amu
TOF repetition rate	--	33 kHz
TOF time resolution	--	30 μ s

Each sediment sample was from a sediment column at a depth of about 2 m, and these columns were taken from the coastal area of Shanghai. Shanghai is a part of the alluvial plain of the Yangtze River Delta, and the offshore sediments are also formed by the impact of the Yangtze River sediment, which can represent the background of the urban surface in Shanghai. Based on the underwater deposition rate of the Yangtze River Delta (around 1-4 cm per year^{1, 2}), these core sediment samples can be dated for about 100 years ago. The metal concentrations and elemental ratios of 28 reference sediments are shown in Table S2 and Table S3, respectively.

Table S2 Metal concentrations of reference sediments in the sampling area.

Sample	Depth (m)	Al (mg/kg)	Ti (mg/kg)	Fe (mg/kg)	Sn (mg/kg)	Pb (mg/kg)	Ce (mg/kg)	La (mg/kg)	Nb (mg/kg)	W (mg/kg)	U (mg/kg)
S1	2.25	54000.0	5025	31780	3.12	21.9	97.7	54.6	16.8	2.39	2.48
S2	2	43623.5	6866	30310	6.62	19.4	79.7	42.8	13.7	1.27	1.53
S3	2	59294.1	4431	31220	3.34	25.7	66.9	36.4	14.6	1.66	2.02
S4	2	66705.9	6118	40460	4.19	25.9	116	63.5	22.5	1.94	2.97
S5	1.9	58764.7	4017	30030	3.58	18.5	64.3	34.1	13.5	1.32	1.75
S6	2.1	42988.2	6681	32130	2.93	17.1	125	67.6	18.7	1.32	2.09
S7	2	50347.1	3408	23310	2.35	15.9	68	37.2	12.8	0.98	1.76
S8	2	48282.4	4844	29050	2.76	20.5	68.5	36.4	13.5	1.43	1.58
S9	1.9	48547.1	4425	26740	2.59	14.5	63.5	34.1	13.5	1.37	1.91
S10	2	59823.5	4661	30870	3.11	25.2	74.2	40	15	1.79	2.37
S11	2	63000.0	4780	33250	3.98	22.9	79.5	43.3	16.2	1.67	2.39
S12	2	73058.8	4613	38640	3.24	25.6	80.7	43.3	16.4	1.92	2.54
S13	2.2	52676.5	4497	27160	2.68	20.3	72.3	39	15.2	1.68	1.94
S14	2.2	71470.6	4461	36190	3.48	21.5	77.5	40.9	16.9	1.75	2.36
S15	2	78352.9	4767	43470	3.92	27.8	83.8	44.4	17.4	2.01	2.45
S16	2.2	70411.8	4348	34790	3.46	21	79.9	42.1	16.3	1.8	2.24
S17	2.1	82058.8	4794	44380	3.55	29.1	80	42	18.4	2.05	2.62
S18	2.1	70941.2	4241	36120	3.73	24	77.4	40.7	15.3	1.69	2.13
S19	2.1	77294.1	4572	39550	3.54	26.9	72.6	38.7	16.9	1.77	2.45
S20	2.1	69882.4	4368	34650	3.44	20.9	68.5	36.6	15.6	1.72	2.25
S21	2	76235.3	4588	41230	4.82	28.9	73.9	39.1	16.2	2.09	2.5
S22	2.1	56647.1	4222	27790	3.54	19.9	78.4	41.8	15.5	1.52	2.18
S23	2.1	80470.6	4699	43680	4.1	30.4	77.8	40.9	17.7	2.03	2.8
S24	2.1	66705.9	4343	34020	3.55	24.1	72.1	38.4	15.8	1.58	2
S25	2.1	80470.6	4583	44170	4.31	30.8	87.5	45.9	16.4	2.2	2.68
S26	2.1	76764.7	4375	37730	3.44	24.2	96.9	51.9	15.6	1.82	2.18
S27	2.1	51405.9	3935	28140	3.77	19.4	64.5	34.2	12.7	1.51	1.67
S28	2	72529.4	4676	38640	3.82	26.6	77.8	41.7	16.5	2.02	2.49

Table S3 Elemental ratios in reference sediments in the sampling area.

	Ti/Nb	Ti/W	Ti/Al	Ti/Fe	Ce/La	W/Nb	Pb/ Nb	Sn/ Nb	W/U
Mean	284±17	2629±374	0.070±0.013	0.133±0.020	1.87±0.02	0.11±0.01	1.46±0.22	0.21±0.03	0.78±0.09
Minimum	261	2083	0.057	0.104	1.83	0.09	0.91	0.16	0.56
Maximum	328	3478	0.100	0.167	1.91	0.13	1.88	0.27	0.96
1 st Quartile	271	2379	0.060	0.116	1.85	0.10	1.29	0.19	0.72
3 rd Quartile	297	2998	0.084	0.152	1.89	0.12	1.60	0.23	0.83
Average crustal ratio	312	1950	0.049	0.111	2.1	0.16	1.42	0.18	0.77

Note: Crustal REEs values are those reported in the study by Rudnick et al.,³ and the average crustal elemental ratios are calculated based on the upper crustal elemental concentrations reported in this study.

Table S4 Results of principle component analysis carried out for source apportionment of metals in sampling sites.

	PC1	PC2	PC3	PC4
Nd	0.984			
Tb	0.981			
Dy	0.980			
Sm	0.979			
Al	0.979			
Gd	0.976			
Ho	0.967			
Pr	0.966			
Tm	0.960			
Er	0.957			
Zr	0.953			
Yb	0.951			
Hf	0.950			
Lu	0.937			
Eu	0.929			
Nb	0.920			
Y	0.919			
Sc	0.890			
La	0.875		0.445	
Ta	0.845			0.443
Th	0.822			0.376
Ce	0.808		0.459	0.331
Ga	0.807		0.572	
Ti	0.786		0.309	
Ag	0.741		-0.343	-0.542
U	0.727	0.379		
Mg	0.628	0.602	-0.417	
Ni		0.970		
V		0.954		
Fe		0.954		
Co		0.953		
Ge	0.333	0.926		
Cu		0.916		
Mn		0.869		
Sr	-0.339	0.860	0.315	
Cr	-0.541	0.806		
Mo	0.445	0.714	0.463	
Pt		-0.697		0.544
Sn			0.934	
Zn	0.439		0.880	
Cd	0.426		0.858	
Pb	-0.516	0.358	0.723	
Ba	0.380	-0.483	0.695	
W	0.461	0.468	0.658	
Cs		-0.444		0.845
Rb		-0.441		0.841
Eigenvalues	25.32	11.13	5.54	2.63
Percentage of variance explained (%)	51.2	22.3	14.0	7.4

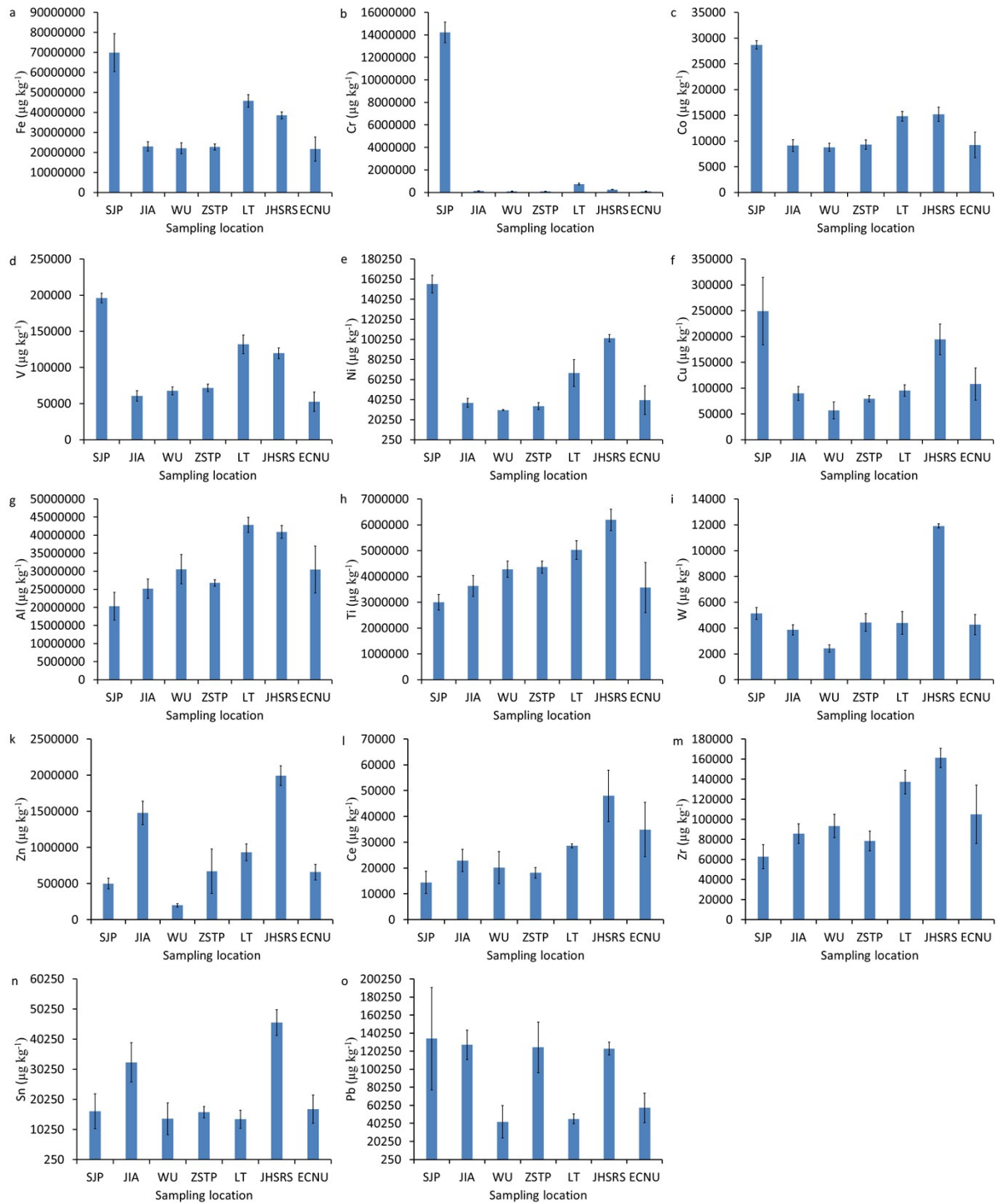


Fig. S1 Selected element concentrations (a) Fe, (b) Cr, (c) Co, (d) V, (e) Ni, (f) Cu, (g) Al, (h) Ti, (i) W, (k) Zn, (l) Ce, (m) Zr, (n) Sn, and (o) Pb.

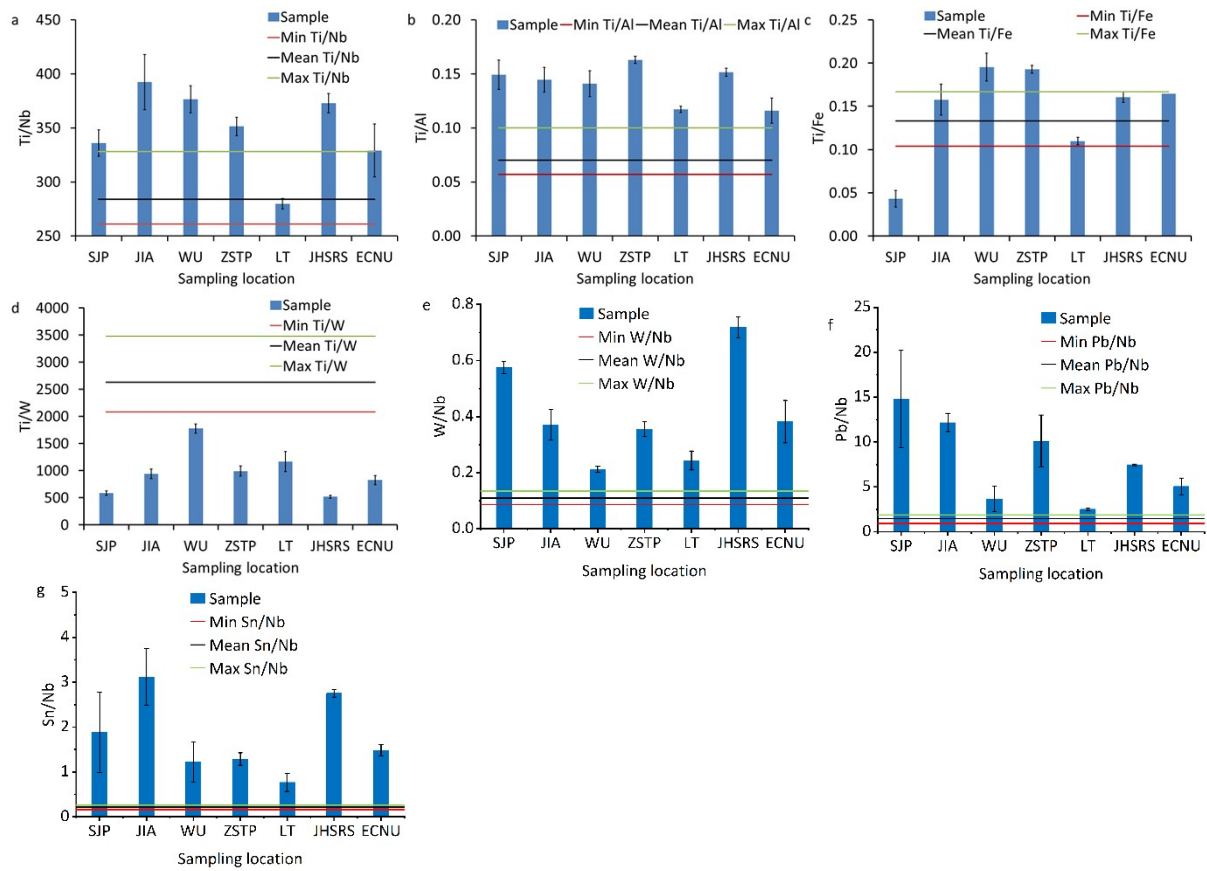


Fig. S2 Elemental ratios of (a) Ti/Nb, (b) Ti/Al, (c) Ti/Fe, (d) Ti/W, (e) W/Nb, (f) Pb/Nb, and (g) Sn/Nb in road dust samples. The line indicates the natural background crustal elemental ratio (minimum, mean, and maximum) of 28 sediments collected in the sampling area.

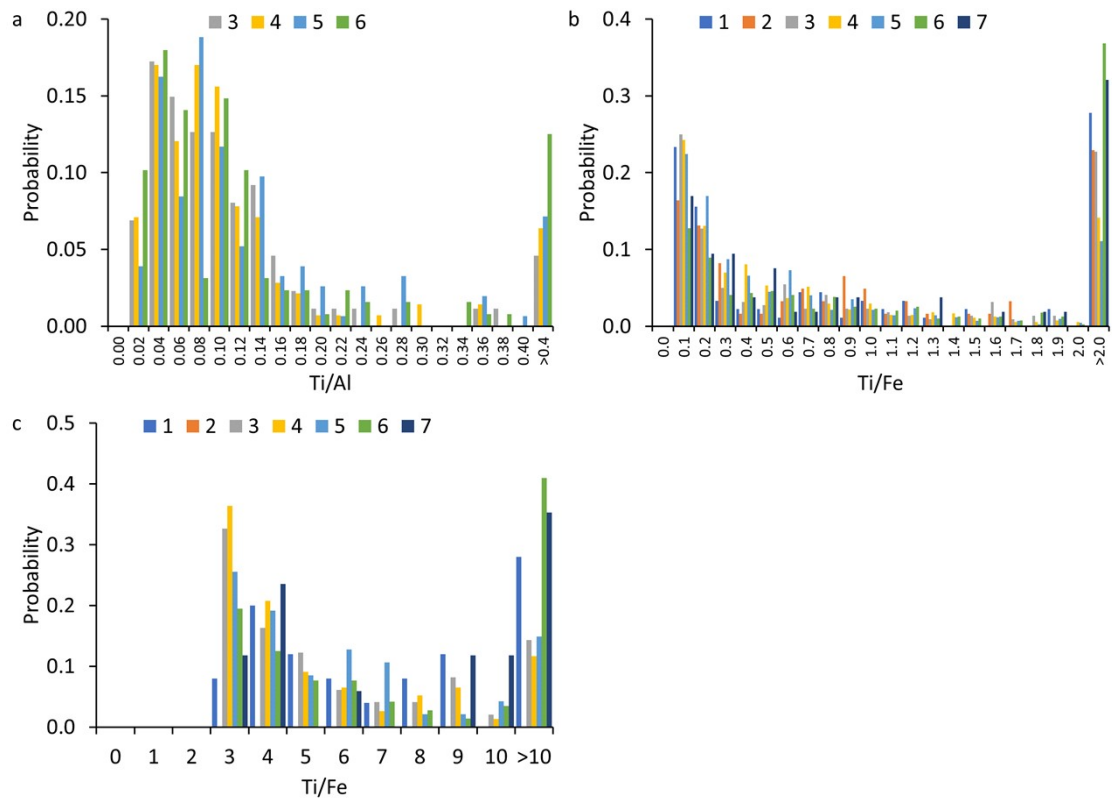


Fig. S3 Elemental ratios of (a) Ti/Al, and (b, and c) Ti/Fe on a single particle basis obtained by SP-ICP-TOF-MS. Samples 1, 2, and 7 contained few Ti- and Al-containing particles that were not sufficient to construct an elemental ratio distribution.

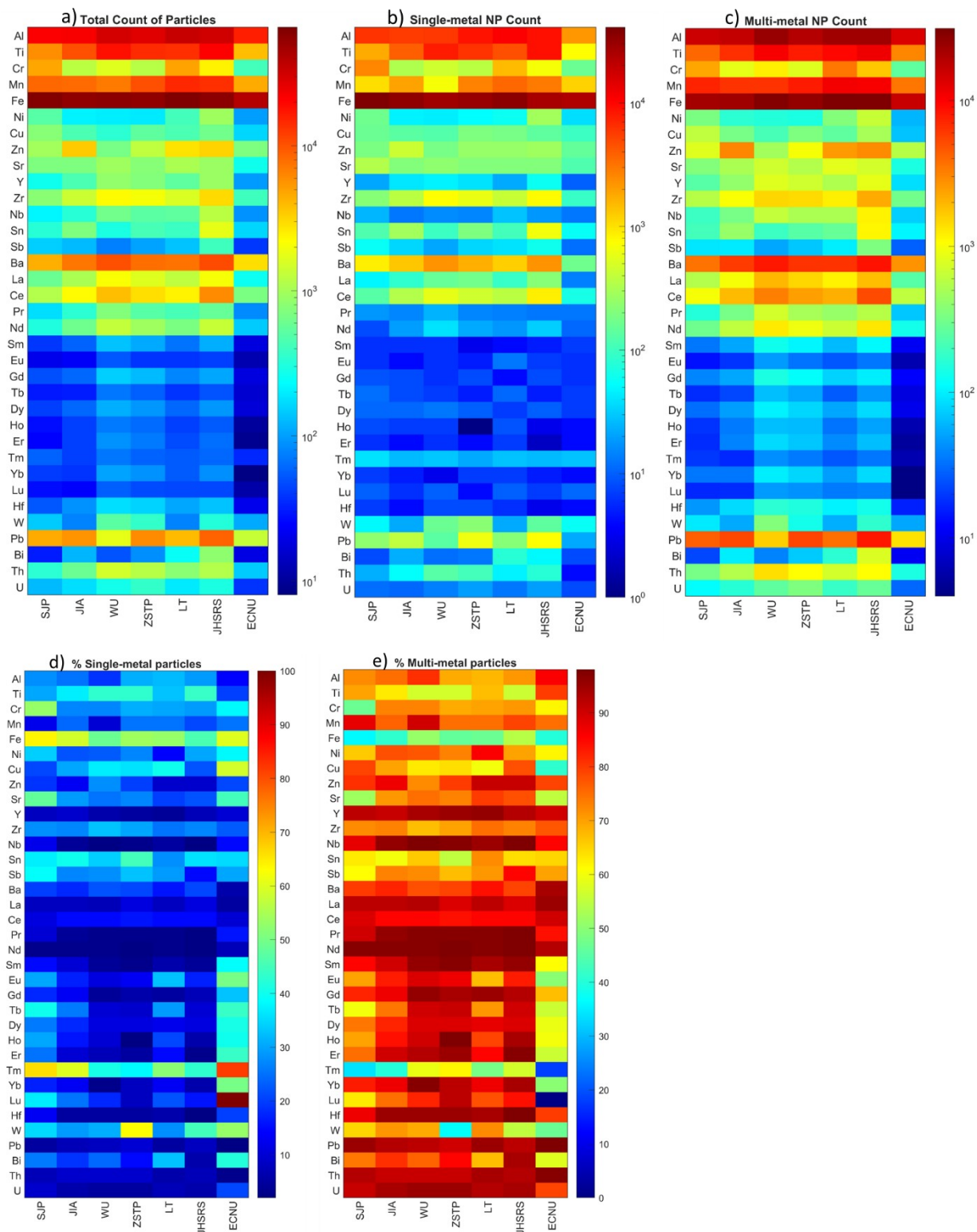


Fig. S4 Number of particles (particles/L) detected by SP-ICP-TOF-MS (a) total number of detected, (b) number of single metal particles, and (c) number of multi-metal particles, (d) percentage relative abundance of single metal particles, and (e) percentage relative abundance of multi-metal particles. All samples were analyzed in triplicates and the triplicate data were merged prior analysis.

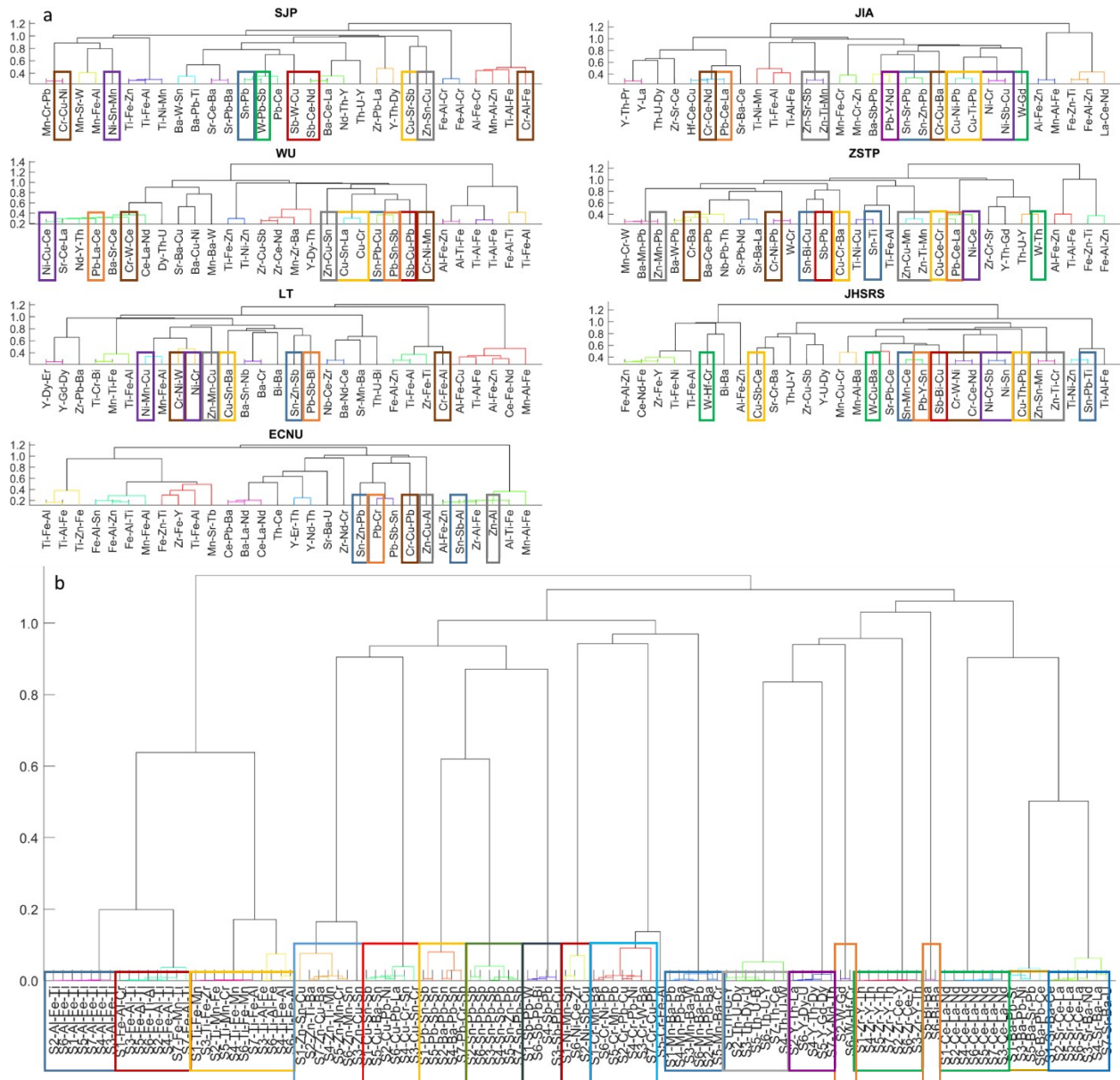


Fig. S5 Dendrogram of intra-sample hierarchical clustering analysis of road dust samples. First and second correlation distance cutoffs were sat at 0.5 and 0.2, respectively and maximum number of first stage clustering was sat at 30. Samples extracted using ultrapure water. Clusters are donated based on the frequency of element occurrence in particles in each cluster and does not necessarily infer mass fraction within particles.

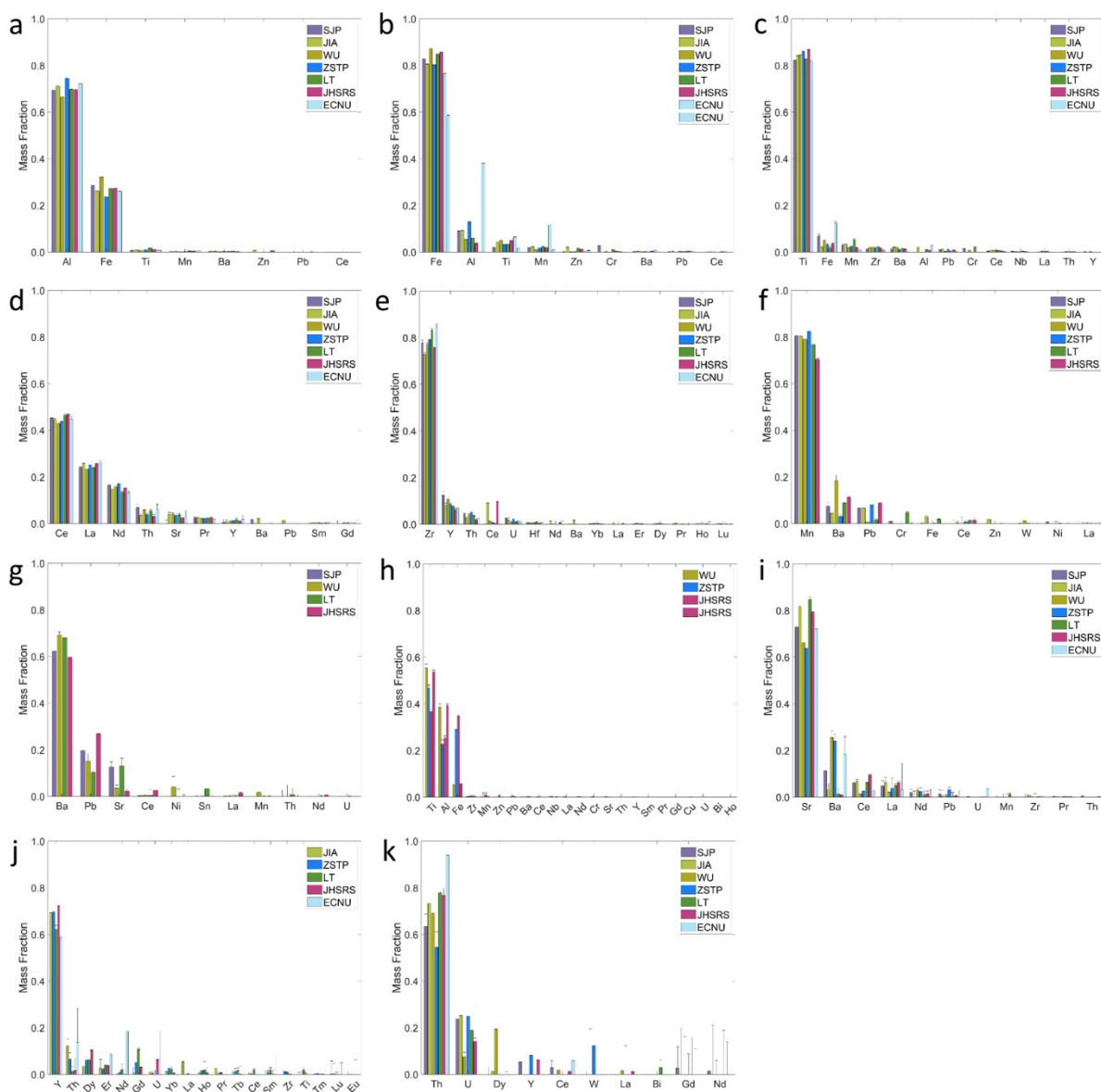


Fig. S6 Mean elemental mass composition of natural mmNP clusters identified in the dust samples (a) Al, (b) Fe, (c) Ti, (d) Ce, (e) Zr, (f) Mn, (g) Ba, (h) Ti, (i) Sr, (j) Y, and (k) Th-rich particles.

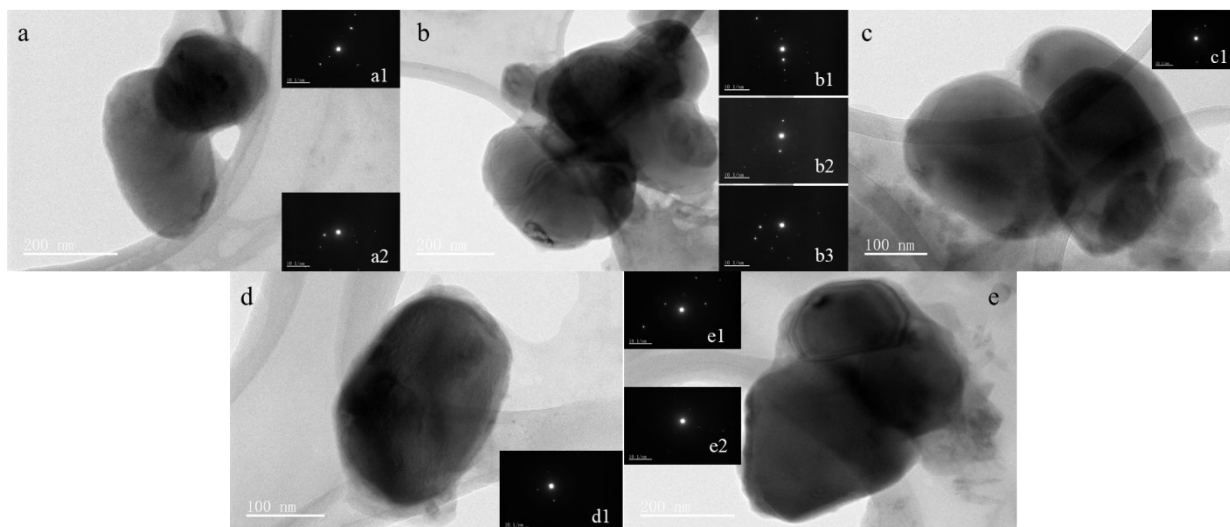


Fig. S7 Other Ti associated particles (a-d: anatase and rutile, e: Magnéli phase of titanium oxides) in dust samples.

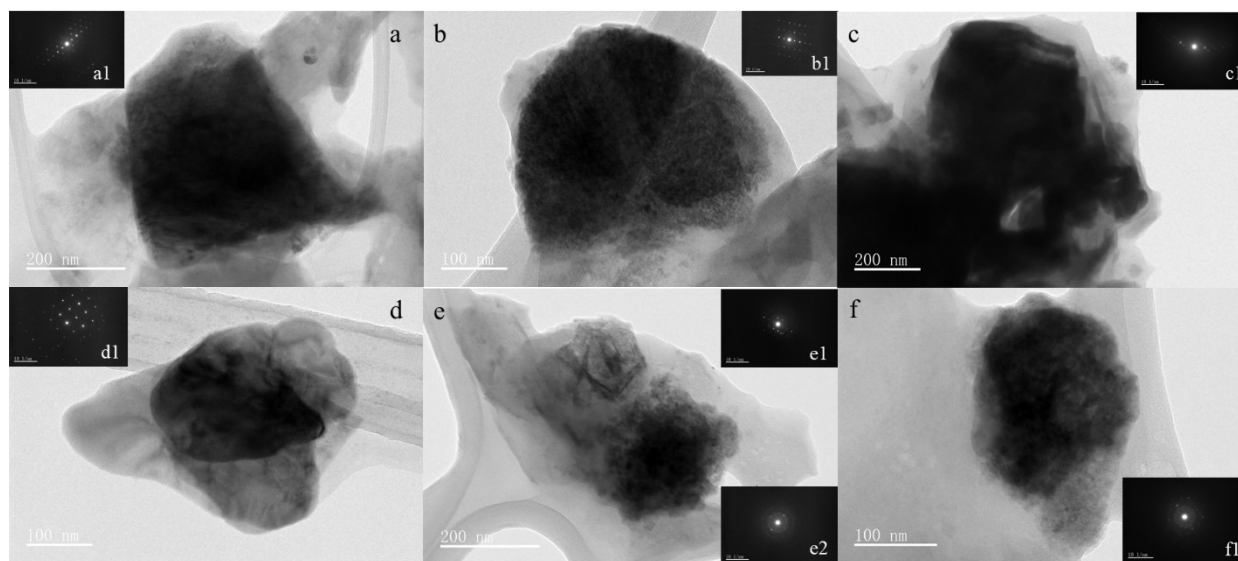


Fig. S8 Fe associated particles (a: ilmenite, b: hematite, c: pyrrhotite, d: magnetite, e: fayalite, f: Fe-Cr oxides) in dust samples, among which, d was found in JHSRS dust and the others were found in SJP dust.

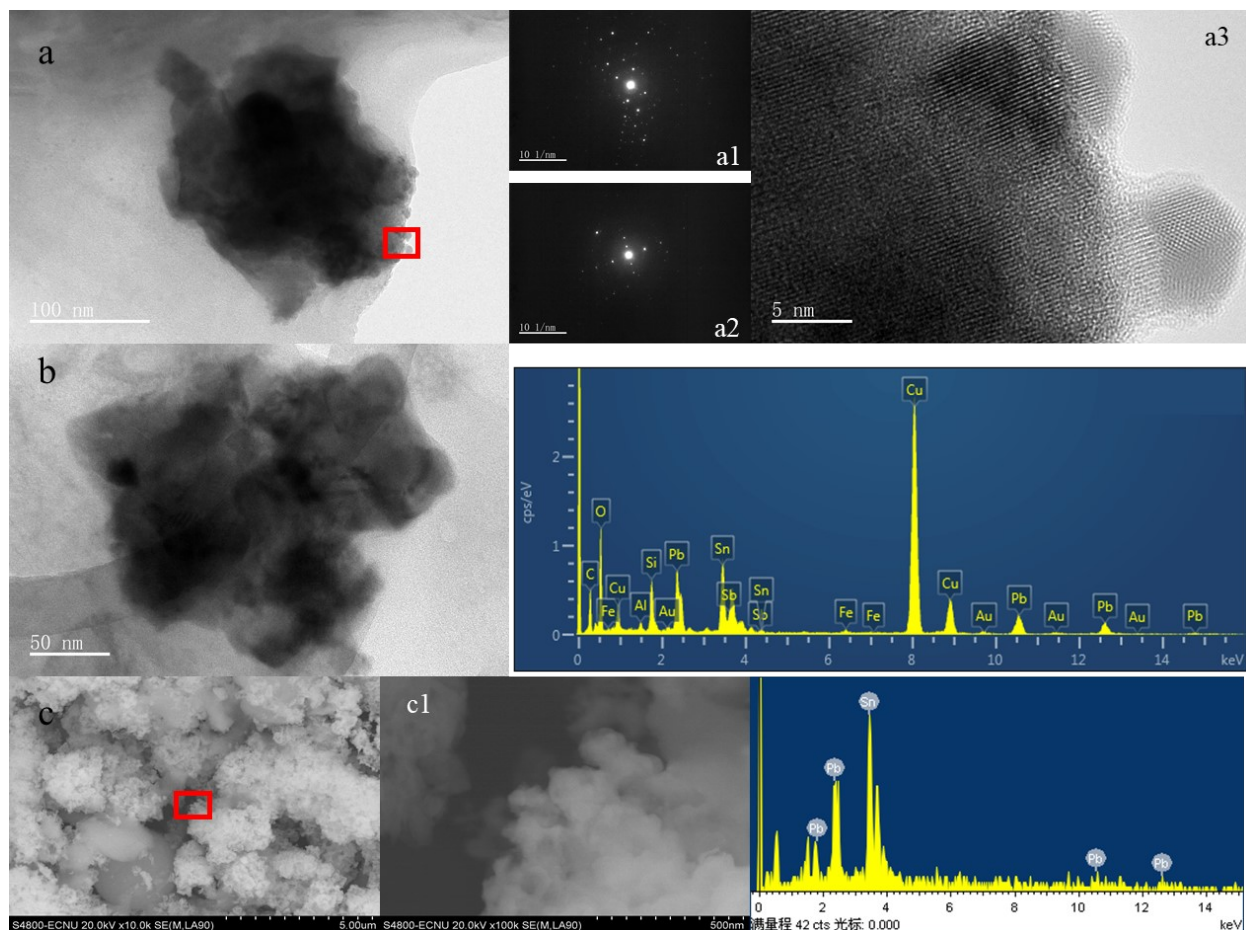


Fig. S9 Co-existence of Pb and Sn in particles of dust samples.

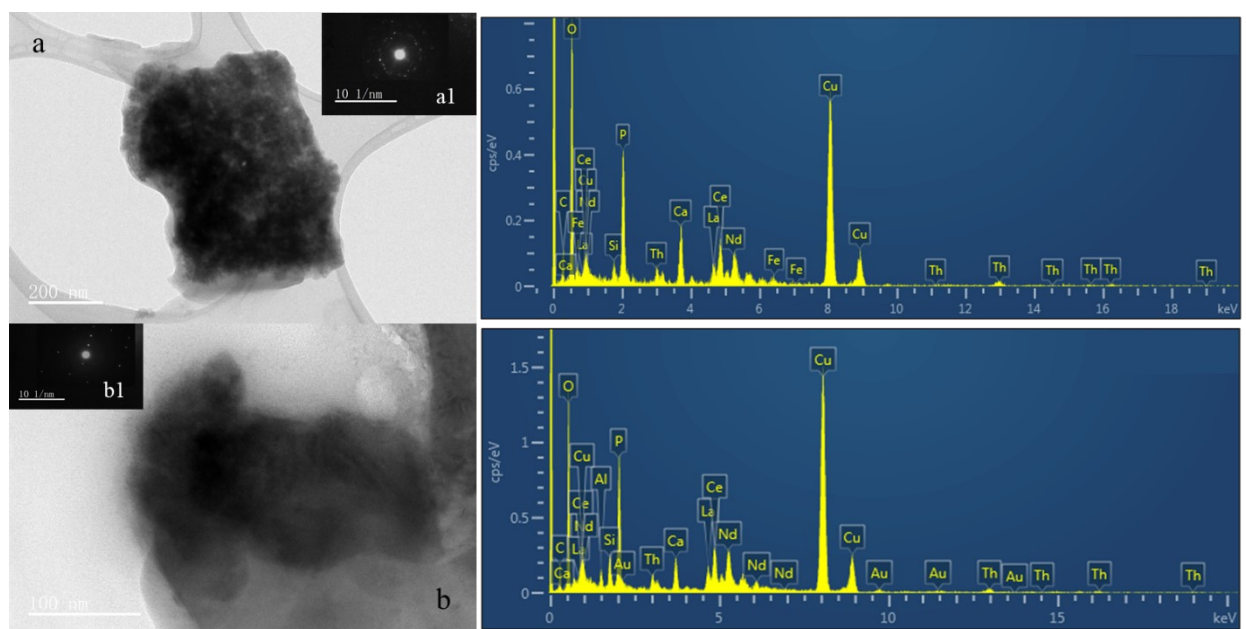


Fig. S10 TEM image shows the co-occurrence of Ce, La, Nd and Th in particles of dust samples.

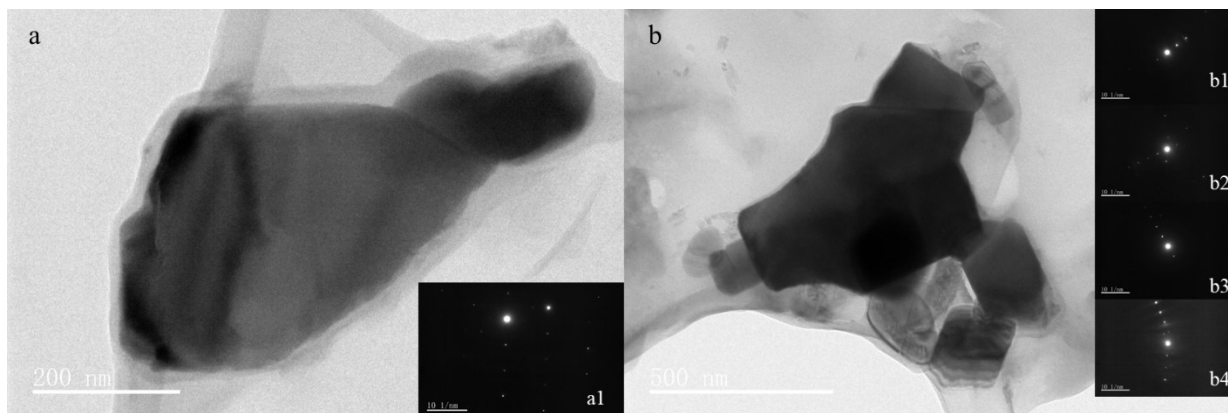


Fig. S11 Zn associated particles (a: zincite, b: aggregation of zincite and smithsonite) found in dust samples.

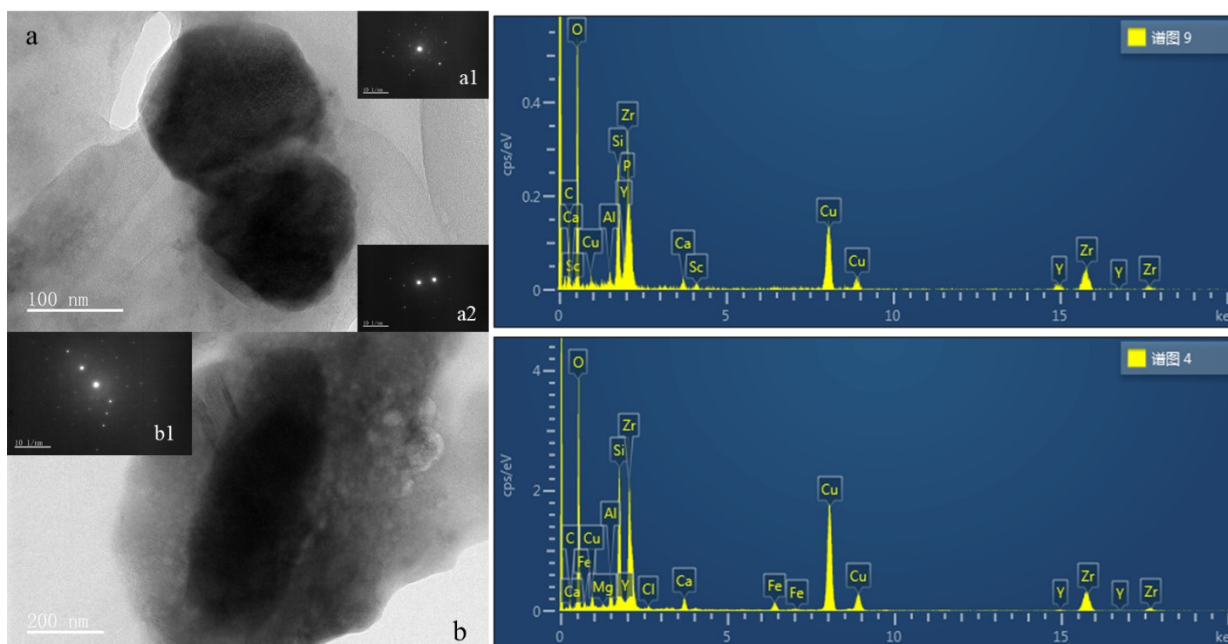


Fig. S12 Zr associated particles (a: Zr-Sc phosphate, b: baddeleyite) found in dust samples.

Reference

1. A. Wang, S. Pan, Y. Zhang and Z. Liu, Modern sedimentation rate of the submarine delta of the Changjiang River, *Marine Geology & Quaternary Geology*, 2010, **30**, 1-6.
2. Q. Ran. Modern sedimentation rates of the Changjiang Subaqueous delta, *Nanjing University*, 2010.
3. R. Rudnick, S. Gao, H. Holland and K. Turekian, Composition of the continental crust, *The Crust*, 2003, **3**, 1-64.